*Pure & Appl. Chem.*, Vol. 64, No. 6, pp. 799–808, 1992.
Printed in Great Britain.


# Investigating the location and distribution of transition metal cations in porous solids by ESE spectroscopy

Z. Levi, K. Matar, A.M. Raitsimring and D. Goldfarb
Dept. of Chemical Physics, Weizmann Institute of Science, 76 100 Rehovot, Israel

Abstract - Electron spin echo methods were applied to characterize the immediate environment and the spatial distribution of paramagnetic transition metal cations in microporous solids. Electron spin echo envelope modulation (ESEEM) induced by framework $^{27}Al$ nuclei was used to investigate the different sites of $Cu^{2+}$ in zeolites X, Y and A. All $Cu^{2+}$ species obtained after complete dehydration showed relatively large isotropic hyperfine interactions with framework Al. This is indicative of a firm interaction of the cation with the framework oxygens. Orientation selective experiments provided additional information concerning the arrangement of the $^{27}Al$ nuclei around the $Cu^{2+}$ and led to site identification. Furthermore, such measurements separated the contributions of distant and near Al nuclei to the modulation.

The immediate environment of $Mn^{2+}$ in MnAlPO-5 where the $Mn^{2+}$ was incorporated during synthesis as compared to post synthesis introduction via impregnation was investigated. ESEEM induced by framework $^{31}P$ and $^{27}Al$ nuclei was used to investigate the location of the $Mn^{2+}$ cations with respect to these framework elements and the spatial distribution of the $Mn^{2+}$ centers throughout the structure was studied by the "2+1" ESE pulse sequence. All the experimental results obtained by these methods led to the conclusion that in MnAlPO-5 the $Mn^{2+}$ is not situated in the framework but is rather bounded to the external surface via terminal framework oxygens.

## INTRODUCTION

Transition metals can be incorporated into zeolites and related materials either as exchangeable extra framework cations or in some special cases as part of the framework. In both cases they play an important role in terms of the catalytic properties of these materials. When the transition metal involved is paramagnetic, electron spin echo (ESE) spectroscopy is a very useful method for investigating the immediate environment of the paramagnetic cations and their distribution. In the following, two such applications will be presented. The first involves aluminosilicate molecular sieves, namely zeolites, where we used electron spin echo envelope modulation (ESEEM) to study the specific interactions of exchangeable $Cu^{2+}$ cations with the framework in zeolites X, Y and A. In hydrated zeolites the cations are mobile and undergo rapid exchange between various sites. Upon dehydration they become localized and coordinate to framework oxygens, therefore they distort the framework geometry and affect the

electron density distribution on the neighboring Si and Al (ref. 1). This causes a broadening of the Si and Al NMR signals, which in turn prevents the detection of the specific cation interactions with the framework in dehydrated zeolites. When the cations are paramagnetic, these fine interactions may be expressed as superhyperfine interactions with framework $^{27}Al$ nuclei and can be investigated by ESEEM. Moreover, the application of orientation selective ESEEM experiments can provide additional information regarding the arrangement of the $^{27}Al$ around the paramagnetic cation and lead to site identification.

The second application involves $Mn^{2+}$ incorporated into aluminophosphate (AlPO-n) molecular sieves. The AlPO-n materials have structural characteristics that are similar to those of zeolites. Some of them have relatively large unidimensional channels (ref. 2) which is an important property for catalytic purposes. The neutrality of their framework, responsible for the absence of Brönsted activity, is, however, a severe limitation. This disadvantage can be circumvented by introducing negative charges into the framework which will in turn require the presence of exchangeable cations and the possibility to create the desired acidity. The incorporation of several transition metal cations such as $Ti^{+}$, $Mn^{2+}$, $Fe^{2+}/Fe^{3+}$ and $Co^{2+}$ into tetrahedral sites in the framework of a number of AlPO-n structures have been reported (ref. 3). We used EPR (X-band and Q-band), ESEEM and "2+1" ESE measurements to investigate the immediate environment of $Mn^{2+}$ and its distribution throughout the structure in MnAlPO-5 after synthesis, calcination, hydration and dehydration. The results are compared to those obtained from $Mn^{2+}$ impregnated onto AlPO-5 and $Mn^{2+}$ exchanged into SAPO-5 (silico-alumino phosphate) where the $Mn^{2+}$ cations do not occupy framework sites.

## EXPERIMENTAL

### Materials and sample preparation

Zeolites NaX (13X, Si/Al=1.25) and NaA (4A, Si/Al=1.0) were purchased from Aldrich. NaY (Si/Al=2.5) was a gift from Conteka, Sweden. $Cu^{2+}$ was introduced by exchange with a $Cu(NO_3)_2$ solution (ref. 4). The exchange level is approximately one $Cu^{2+}$ cation per 7 and 40 unit cells for X and Y zeolites, and A zeolite respectively. Dehydration was carried out by slowly heating the sample (50°/h) under vacuum to the desired dehydration temperature at which the sample was left under a residual pressure of $10^{-5}$ torr for ~16h. Most of the samples dehydrated above 300°C were exposed to 400 torr oxygen for 2h, at the dehydration temperature, to oxidize any $Cu^{1+}$ or $Cu^{0}$ formed during the dehydration process. The oxygen was then pumped off and the samples were sealed. We shall refer to oxidized samples in the text as Cu-NaX (400°C, $O_2$) indicating that the sample was dehydrated at 400°C and oxidized.

MnAlPO-5, AlPO-5 and SAPO-5 were synthesized as described in the literature (ref. 5). The as-synthesized materials were calcined in flowing air at 550°C. The calcined samples were then left open to adsorb water, so that all calcined samples we refer to are hydrated. $Mn^{2+}$ was impregnated onto calcined AlPO-5 by stirring AlPO-5 with a solution of Mn $(CH_3COO)_2$ at 94°C until evaporation. Calcined SAPO-5 was exchanged with a Mn $(CH_3COO)_2$ solution at 70°C for 24h. The composition of the samples used in this study are given in Table 1. The synthesis products were characterized by powder X-ray diffraction (ref. 6) and $^{31}P$ and $^{27}Al$ MAS NMR (ref. 7). Dehydration was done as in the zeolite samples. Frozen glassy water/glycerol solutions of $MnSO_4$ were employed as a model system for samples with a random distribution of paramagnetic centers. The spin concentration of $Mn^{2+}$ in the solutions was varied between $3 \cdot 10^{18}$ - $10^{19}$ $cm^{-3}$.

TABLE 1. Compositions of the MnAlPO-5 samples studied[a]

| Sample | Atom ratio | | | |
|---|---|---|---|---|
| | Al: | P: | Mn: | Si: |
| MnAlPO-5(1) | 0.985 | 1 | 0.0042 | - |
| MnAlPO-5(3) | 1.16 | 1 | 0.0005 | - |
| MnAlPO-5(4) | 1.36 | 1 | 0.002 | - |
| Mn-AlPO-5 | 1.13 | 1 | 0.0056 | - |
| Mn-SAPO-5 | 1.15 | 1 | 0.0037 | 0.2045 |

[a]Chemical analysis was obtained by the ICP method.

#### Instrumentation and spectroscopic measurements

ESR measurements were performed on a Varian E-12 spectrometer at X-band ($\approx$ 9 GHz) and Q-band ($\approx$ 35 GHz). The spectra were recorded at 150K and at room temperature (RT). ESEEM measurements were performed at 4K using a home built spectrometer (ref. 8). Two-($\pi/2-\tau-\pi-\tau$–echo) and three-pulse ($\pi/2-\tau-\pi/2-T-\pi/2-\tau$–echo) ESEEM experiments were performed with the appropriate phase cycling to eliminate unwanted echoes (ref. 9). The "2+1" sequence (ref. 10) is similar to the two-pulse sequence where a third, "+1", pulse is introduced in between the two pulses. In this experiment the interval $\tau$, between the first and the last pulse, is held fixed and the echo amplitude is recorded as a function of the time interval between the first and the "+1" pulse. To generate the "+1" pulse an additional microwave channel with the possibility of independently changing the amplitude, phase and duration of the "+1" pulse was used. The relative amplitudes of the "+1" and the first (last) pulse, $H_1^+/H_1$, could be varied between 0 and 3, and the minimum length of the additional pulse was 20 ns. The usual procedure of a four step phase cycling (ref. 9) was used to eliminate unwanted ESE signals.

## RESULTS AND DISCUSSION

#### $Cu^{2+}$ doped X, Y and A zeolites

Complete dehydration of Cu-NaX (400°C, $O_2$) generates a major $Cu^{2+}$ species termed species A and a minor species termed A'. Their EPR parameters are listed in Table 2. The FT-ESEEM spectrum of species A consists of three major peaks at 2.6, 3.5 and 5.3 MHz (ref. 12). The 3.5 MHz peak, which corresponds to the $^{27}$Al Larmor frequency, $\omega_I$, is due to Al nuclei situated at distances >0.5 nm from the $Cu^{2+}$. These nuclei interact with the $Cu^{2+}$ cation only via weak dipolar interactions and will thus be referred to as distant Al. The other two lines are assigned to first shell $^{27}$Al nuclei and belong to a hyperfine pair split by 2.7 MHz. The first shell $^{27}$Al nuclei are situated at 0.31-0.34 nm (ref. 12) from the $Cu^{2+}$ cation and are the first neighbors of the framework oxygens to which the $Cu^{2+}$ is coordinated. The assignment of the 2.6 and 5.3 MHz lines to a hyperfine pair was based on the dependence of their relative intensities (in the three-pulse FT-ESEEM spectrum) on the time interval $\tau$ (ref. 11).

Dehydrated Cu-NaA and Cu-NaY (400°C, $O_2$) consist of a single species each (D and F respectively) with rather similar EPR parameters as listed in Table 2. The FT-ESEEM spec-

TABLE 2. List of the zeolites investigated, the $Cu^{2+}$ species generated, and their corresponding EPR parameters.

| Zeolite | treatment | species | $g_{\|}$ ($\pm 0.005$) | $g_{\perp}$ ($\pm 0.005$) | $A_{\|}$ ($\pm 5 \cdot 10^{4}$) ($cm^{-1}$) |
|---|---|---|---|---|---|
| Cu-NaX | 400°C | A | 2.35 | 2.062 | $153 \cdot 10^{-4}$ |
| Cu-NaX | 400°C, $O_2$ | A | 2.35 | 2.062 | $153 \cdot 10^{-4}$ |
| | | A' | 2.37 | ~2.06 | $139 \cdot 10^{-4}$ |
| Cu-NaA | 400°C, $O_2$ | D | 2.37 | 2.065 | $145 \cdot 10^{-4}$ |
| Cu-NaA | 400°C, $O_2$ | G | 2.31 | ~2.07 | $163 \cdot 10^{-4}$ |
| | + MeOH | | | | |
| Cu-NaY | 400°C, $O_2$ | F | 2.36 | ~2.07 | $145 \cdot 10^{-4}$ |

trum of Cu-NaA shows a doublet at 2.5 and 5.1 MHz and a line at 3.5 MHz which we assign as in Cu-NaX. In this case, however, additional features at 3 and 4 MHz are observed as well (ref. 4). The FT-ESEEM spectrum of species F in Cu-NaY is similar to that of species D in Cu-NaA, it shows a doublet at 2.6 and 5.2 MHz and the Larmor frequency line. The latter has a relatively weaker intensity as the Al content is significantly lower.

Adsorption of methanol onto dehydrated Cu-NaA (400°C, $O_2$) induces changes in the EPR spectrum (Table 2) indicating a change in the location and/or coordination sphere of the $Cu^{2+}$. The FT-ESEEM spectrum of this newly formed species, G, consists of three peaks at 1.5, 3.5 and 6.1 MHz. As in the previous cases we assign the lines at 1.5 and 6.1 MHz to an hypefine doublet split by an isotropic constant of $4.6 \pm 0.2$ MHz originating from first shell Al.

The relatively high $^{27}Al$ isotropic hyperfine constants found for $Cu^{2+}$ in the dehydrated zeolites investigated indicates that the coordination has some covalent character leading to a finite spin density on the Al nuclei (ref. 13). This is an indication to a firm interaction with the framework. The variation in the size of the isotropic hyperfine constant is related to differences in the site geometry which in turn affects the $Cu^{2+}$ orbitals configuration and their overlap with the oxygen/aluminium orbitals. This is most pronounced in Cu-NaA adsorbed with methanol where the largest hyperfine splitting has been observed. In this case it was found that the $Cu^{2+}$ is coordinated to framework oxygens and to a single methanol molecule (ref. 14). Hence, the symmetry of the $Cu^{2+}$ species is different than in the fully dehydrated samples leading to a larger spin density on the $^{27}Al$ nuclei.

In order to obtain additional information concerning the geometry of the $Cu^{2+}$ sites we carried out orientation selective ESEEM experiments (ref. 8,15,16). In these experiments one makes use of the large $g$-anisotropy of the $Cu^{2+}$ cation and of the limited band-width of the microwave pulse to excite only crystallites with selected orientations. These orientations are determined by the resonant magnetic field, $H_0$, at which the ESEEM experiment is performed. Fig. 1 shows the three pulse FT-ESEEM spectra of Cu-NaA and Cu-NaY (400°C, $O_2$) as a function of the magnetic field. In these experiments $\tau$ was chosen to maximize the doublet intensity with respect to the $\omega_I$ peak. For both materials the spectra are practically field independent. Similar behavior was observed for the two pulse FT-ESEEM spectra.

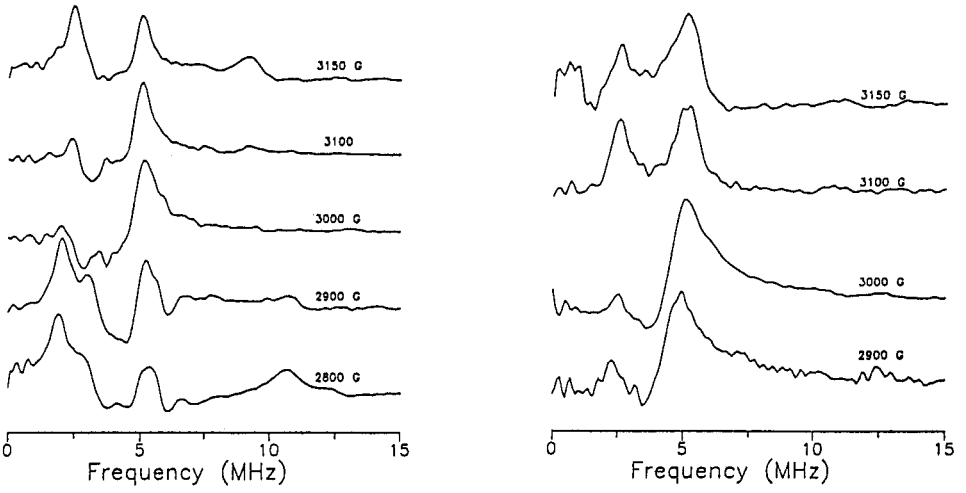


Figure 1: Three pulse (cosine) FT-ESEEM spectra of Cu-NaA (400°C, $O_2$) (left) and Cu-NaY (400°C, $O_2$) (right) recorded at different resonant magnetic fields ($\tau$=0.22 $\mu$s).

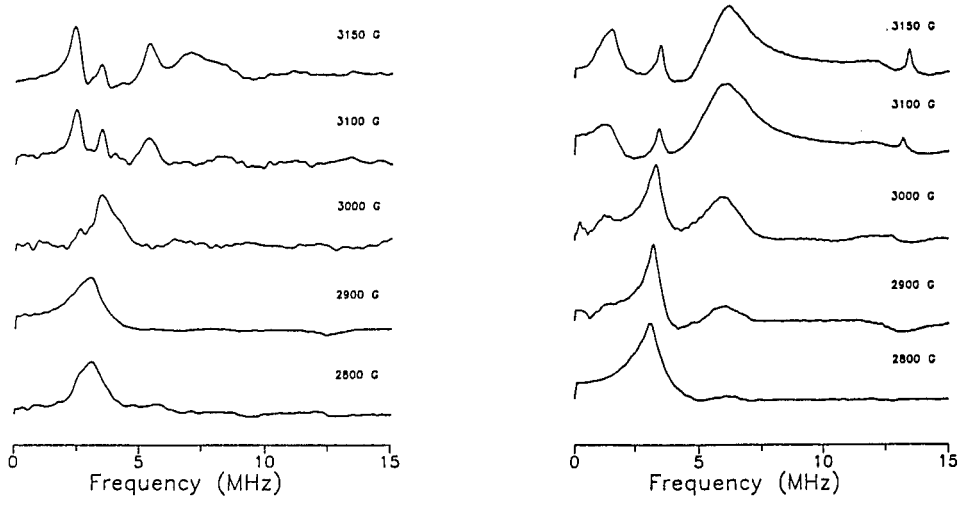


Figure 2: Three pulse (cosine) FT-ESEEM spectra of Cu-NaX (400°C, $O_2$) (left) and Cu-NaA (400°C, $O_2$) after methanol adsorption (right) recorded at different resonant magnetic fields ($\tau$=0.22 $\mu$s).

Although species A in Cu-NaX exhibit a hyperfine splitting rather similar to that of species D and F the field dependence of its FT-ESEEM spectrum is significantly different, as shown in Fig. 2. The spectrum obtained at 3150 G ($g_\perp$ region) shows both the hyperfine doublet and the $\omega_I$ line but as the magnetic field decreases and approaches the $g_\parallel$ region the relative intensity of the doublet decreases and the $\omega_I$ line dominates the spectrum. Similar behavior is exhibited by species G in Cu-NaA after methanol adsorption (Fig. 2).

The field dependence of the doublet intensity can be explained in terms of the anisotropy of the modulation amplitudes and the site geometry. The modulation amplitudes are determined by the probabilities of the allowed and forbidden EPR transitions connecting the nuclear spin manifolds (ref. 17). The mixing of the nuclear states leading to the forbidden transitions, is mainly due to the anisotropic hyperfine interaction. Thus the transition probability strongly depends on the orientation of the external magnetic field with respect to the principal axis of the hyperfine tensor. For instance, the modulation amplitude is zero

when the direction of the magnetic field coincides with one of the cannonical orientations of the hyperfine tensor. The vanishing of the doublet when $H_0$ coincides with the $g_{||}$ direction indicates that the principal axes of the hyperfine tensors of all first shell Al are perpendicular to the principal direction of the g tensor. Fig. 3 shows a schematic representation of a cation site in the vicinity of a six ring, which is the most common cation site in zeolites X, Y and A. A $Cu^{2+}$ cation located in the plane of the ring would exhibit the field dependence observed experimentally, assuming that the principal axis of the g tensor coincides with the local symmetry axis of the site and that the principal axis of the hyperfine interaction lies approximately along the Cu-Al axis. When the Al quadrupole interaction is not negligible, the modulation amplitudes are not determined solely by the orientation of the anisotropic hyperfine but are affected by the orientation of the quadrupole tensor as well. In dehydrated zeolites the quadrupole interaction is large (ref. 18) causing additional broadening of all the ENDOR transitions due to the orientational disorder. The $|1/2> - |-1/2>$ transition, is however, less affected as it depends on the quadrupole interaction only to second order thus it is expected to dominate the FT-ESEEM spectrum. In this case the modulation amplitudes are expected to be determined mostly by the direction of the external field with respect to the hyperfine principal axis. Hence we conclude that in species A and G the $Cu^{2+}$ is situated close to the ring plane. Since the doublet corresponding to first shell Al in Cu-NaA and Cu-NaY do not disappear at low fields we deduce that in species D and F the $Cu^{2+}$ lies above or below the ring plane.

The $\omega_I$ line, corresponding to the distant Al, does not show any field dependence, because, unlike the first shell Al, their arrangement about the $Cu^{2+}$ approaches a spherical distribution. Therefore, at any magnetic field orientation there will be enough Al nuclei to induce significant modulation at the Larmor frequency. Consequently, this line will not be suppressed as the $g_{||}$ region is approached. Actually, this line may even be enhanced as at lower fields, where the Zeeman interaction is smaller, the transition probability of the forbidden transitions increases.

**MnAlPO-5**

The Q-band EPR spectra of as-synthesized MnAlPO-5, calcined Mn-AlPO-5, impregnated Mn-AlPO-5 and exchanged Mn-SAPO-5 are rather similar as shown in Fig. 4. This suggests

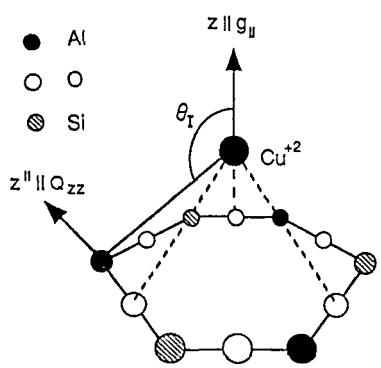


Figure 3: A schematic description of a $Cu^{2+}$ site in zeolites X, Y and A involving a characteristic six ring site.

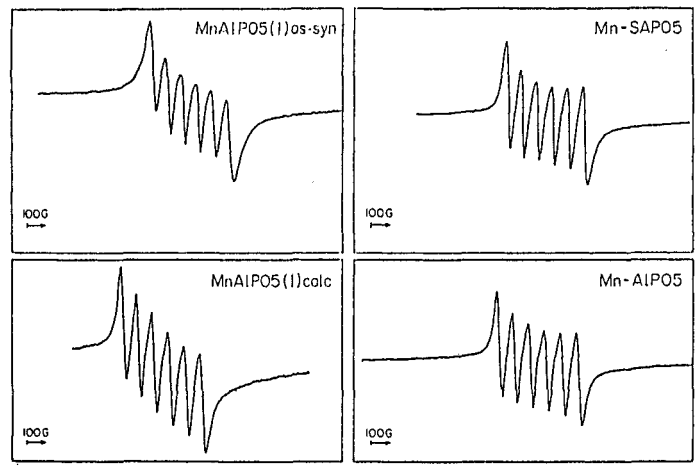


Figure 4: Q-band spectra of as-synthesized MnAlPO-5(1), calcined MnAlPO-5(1) impregnated Mn-AlPO-5 and Mn-SAPO-5 recorded at 25°C.

that the local environment of the $Mn^{2+}$ in all four samples is similar. ESE experiments can provide additional specific information about this local environment. In the case of aluminophosphate molecular sieves one can make use of the modulation from both framework Al and P to probe the surroundings of the $Mn^{2+}$. $^{31}P$ modulation is more attractive since for $^{31}P$ I=1/2 and the ESEEM analysis is relatively simple. For $^{27}Al$, where I=5/2, the quadrupole interaction complicates the analysis considerably. The $^{31}P$ modulation has however, the disadvantage of being rather shallow.

Figure 5 shows the three-pulse ESEEM of as-synthesized MnAlPO-5, impregnated Mn-AlPO-5 and exchanged Mn-SAPO-5 obtained at $\tau$=0.26 $\mu$s, where the Al modulation is suppressed and the $^{31}P$ modulation depth maximized. The corresponding FT-ESEEM spectra (magnitude mode) show a single peak at the $^{31}P$ Larmor frequency. The modulation is very shallow and is similar in the first two samples. In Mn-SAPO-5 the modulation is even shallower.

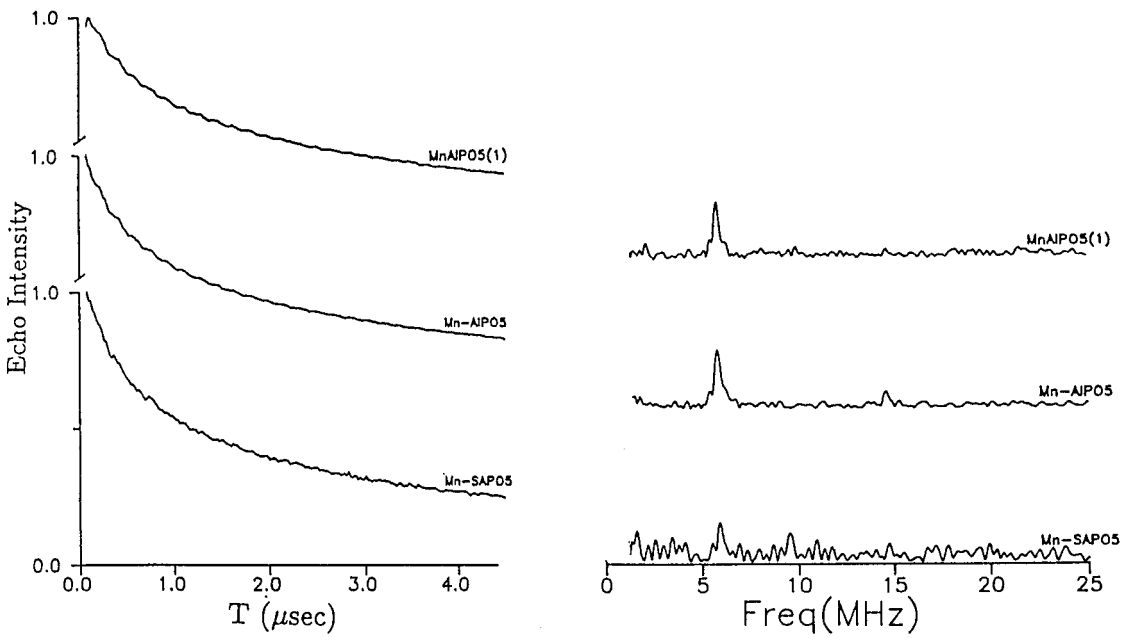


Figure 5: Three pulse ESEEM of MnAlPO-5(1), Mn-AlPO-5 and MnSAPO5 along with the corresponding FT-ESEEM spectra (magnitude) recorded at $H_0$=3430 G, $\tau$=0.26 $\mu$s.

This is expected since part of the P is replaced by Si, so less $^{31}P$ nuclei contribute to the modulation. The single peak at the Larmor frequency indicates that the isotropic hyperfine constant is zero and that the Mn-$^{31}P$ interaction is a weak dipolar interaction. The similarity of the EPR spectra and of the modulation depth of Mn-AlPO-5 and MnAlPO-5 suggest that the $Mn^{2+}$ in MnAlPO-5 does not occupy framework sites. In impregnated Mn-AlPO-5, the Mn-$^{31}P$ distance can, in principle, be close to that of framework $Mn^{2+}$ substituting Al, but considering the structure of AlPO-5 the maximum number of $^{31}P$ nuclei surrounding the $Mn^{2+}$ at this distance is three. In a framework site the $Mn^{2+}$ is surrounded by four $^{31}P$ nuclei and a deeper modulation is expected.

We calculated the expected modulation pattern from framework $Mn^{2+}$substituting Al, taking into account a tetrahedral arrangement of $^{31}P$ nuclei at a distance of 0.31 nm (ref. 19) using the point dipole approximation. The calculated ESEEM, multiplied by a decaying exponent to acount for relaxation, is shown in Fig. 6. The experimental ESEEM is significantly

shallower than the calculated trace indicating a larger interaction distance and/or a smaller number of interacting $^{31}P$ nuclei. The experimental results agree better with the middle trace in Fig. 6 which was obtained with 6 $^{31}P$ nuclei at an averaged distance of 0.5 nm, calculated using the spherical model approximation (ref. 20). It should, however, be noted that the ESEEM simulations were done under the assumption that the $Mn^{2+}$ can be treated as a pseudo S=1/2 system and that the zero field splitting is small enough such that the $|1/2>$, $|-1/2>$ state mixing is small and does not affect the modulation.

Additional evidence for the location of the $Mn^{2+}$ in extra-framework sites in MnAlPO-5 was obtained from the EPR spectra of dehydrated samples. Removal of the water at room temperature in calcined MnAlPO-5 broadens the hyperfine lines. Further increases in the dehydration temperature (to 400°C) causes considerable lose of resolution and a narrowing of the whole spectral envelope (ref. 21). These changes are attributed to an increase in the spin exchange interaction due to a decrease in the $Mn^{2+}$-$Mn^{2+}$ distances. The changes are reversible and exposure of the dehydrated sample to water regenerated the original spectrum. This variation in the $Mn^{2+}$-$Mn^{2+}$ distance as a consequence of dehydration indicates that at least part of the $Mn^{2+}$ cations are not situated in the framework which agrees with our previous observations.

The distribution of the $Mn^{2+}$ species within the structure and its dependence on the $Mn^{2+}$ content was investigated by the "2+1" echo sequence. This pulse sequence was specifically designed to study the spatial distribution of paramagnetic centers (ref. 10). It is based on the analysis of the echo decay kinetics, which in this particular experiment is determined exclusively by the dipole dipole interaction between the paramagnetic centers. The decay is a consequence of the so-called "instantaneous diffusion" mechanism (ref. 22). This mechanism originates from electron spin flips induced by the microwave pulses because the dipolar field is "instantaneously" changed if spins are turned by the pulse. Therefore, the decay depends on both the dipolar interaction and on the probability of the spin flip. The spin flip, in turn, depends on the duration and amplitude of the pulses and on the EPR lineshape.

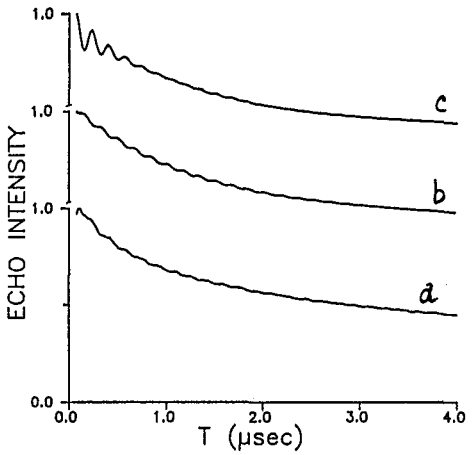


Figure 6: Calculated three-pulse ESEEM for a model of $Mn^{2+}$ surrounded by a) four $^{31}P$ nuclei in a tetrahedral arrangement at a distance of 0.31 nm, b) six $^{31}P$ nuclei spherically distributed around the $Mn^{2+}$ at a distance of 0.5 nm. c) Experimental ESEEM of as-synthesized MnAlPO-5(1) ($\tau$=0.26 $\mu$s, $H_0$=3430 G).

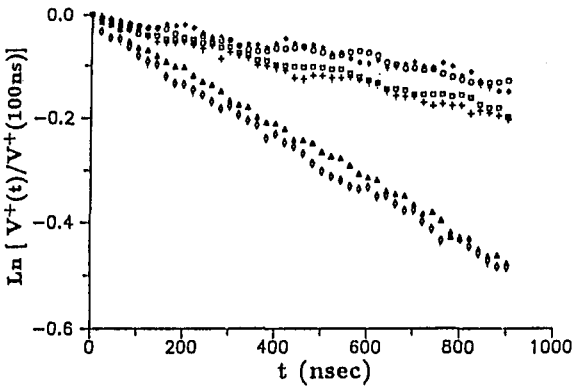


Figure 7: The electron spin echo decays of $Mn^{2+}$ in the various AlPO-5 samples studied.
(0) - MnAlPO-5(3); (*) - MnAlPO-5(4);
(□) - MnAlPO-5(1); (+) - calcined MnAlPO-5(1);
(◇) - impregnated Mn-AlPO-5;
(Δ) - $Mn^{2+}$ in water/glycerol solution ($10^{19}$ $cm^{-3}$).
The value of <SC> in all cases is equal to $\sim 10^{-2}$.

TABLE 3. The average concentrations of $Mn^{2+}$ and the concentration of randomly distributed spins as determined by the "2+1" ESE experiment

| Sample | Average $Mn^{2+}$ concentration $10^{18}$, $cm^{-3}$ | Concentration of randomly distributed spins $10^{18}$, $cm^{-3}$ |
|---|---|---|
| [a]MnAlPO-5(1) | 38.5 | 4[b] |
| MnAlPO-5(1) calc. | 38.5 | 4 |
| [a]MnAlPO-5(4) | 18.3 | 3 |
| [a]MnAlPO-5(3) | 3.7 | 3 |
| Mn-AlPO-5 | 51.3 | 10 |

[a] as-synthesized samples. [b]The error in determining the randomly distributed spin concentration is approximately 20%.

In the case of randomly distributed paramagnetic centers the echo decay is given by (ref. 10):

$$\ell n\, V(t) \cong -2kCt < SC > \qquad (1)$$

C is the concentration of the paramagnetic centers, k is a constant (for $Mn^{2+}$, (S=5/2), $k=2.77\cdot10^{12}$ $cm^3$ $s^{-1}$) and <SC> is a scaling factor related to the spin flip probability. <SC> can be calculated from the experimental conditions, namely the pulse amplitudes, durations and lineshape of EPR signal. Accordingly, once <SC> has been calculated, $C$ can be determined from the echo decay.

As a control, we applied the "2+1" sequence to a series of $Mn^{2+}$ in water/glycerol solutions. The measurements were done at different values of <SC> and the solutions' concentrations were determined using eq. (1). The determined concentrations, in the range $3\cdot10^{18}$-$10^{19}$ $cm^{-3}$, were all within 10% of the known concentrations (ref. 21). The "2+1" echo decays of $Mn^{2+}$ in the different AlPO-5 materials studied are shown in Fig. 7 along with that of a $Mn^{2+}$ in a water/glycerol solution. From the slopes of these decays we calculated the amount of randomly distributed $Mn^{2+}$ species in the sample. The concentrations measured as compared to those obtained by means of chemical analysis are listed in Table 3. The values obtained from these two methods are comparable only for MnAlPO-5(3), which has the lowest $Mn^{2+}$ content, namely $3\cdot10^{18}$ $cm^{-3}$. As the $Mn^{2+}$ content increases the percentage of the randomly distributed ions decreases. For example, in MnAlPO-5(1) the echo decay correspond only to 10% of the average concentration. The calcination is found not to alter the $Mn^{2+}$ distribution within the experimental error limits. $Mn^{2+}$ in the impregnated sample shows a higher degree of random distribution than the as-synthesized MnAlPO-5 with about the same $Mn^{2+}$ content.

These results lead to the conclusion that the distribution of $Mn^{2+}$ ions in as-synthesized MnAlPO-5 is inhomogeneous. Part of the $Mn^{2+}$ cations are randomly distributed whereas the rest forms enriched islands with an $Mn^{2+}$-$Mn^{2+}$ separation not larger than 1-1.5 nm. The latter does not contribute to the ESE signal due to fast relaxation. The "2+1" ESE results are in agreement with the assignment of most of the $Mn^{2+}$ in MnAlPO-5 to extraframework sites.

The similar behavior of impregnated Mn-AlPO-5 and calcined MnAlPO-5 along with the spatial distribution results suggest that most of the "enriched" $Mn^{2+}$ islands are located on the external surface of the AlPO-5 microcrystals coordinated to terminal oxygens and to "external" ligands such as water or OH groups. In this case dehydration causes dehydroxylation followed by some condensation of the $Mn^{2+}$ species enhancing their spin exchange interaction.

## REFERENCES


1. G. Engelhardt and D. Michel. High Resolution Solid State NMR of Silicates and Zeolites, p. 256, John Wiley and Sons (1987).
2. S.T. Wilson, B.M. Lok, C.A. Messina, T.R. Cannan and E.M. Flanagan. J. Am. Chem. Soc. 104, 1146 (1982).
3. E.M. Flanigan, B.M. Lok, R.L. Patton and S.J. Wilson. New Developments in Zeolite Science Technology, p. 103, Proceedings of the 7th International Zeolite Conference, Eds. Y. Murakami, A. Ijima and J.W. Ward, Kodansha, Tokyo (1986).
4. D. Goldfarb and L. Kevan. J. Magn. Reson. 82, 270 (1989).
5. T.S. Wilson and E.M. Flanigen. US Pat. 4567029 (1986); T.S. Wilson, B.M. Lok and E.M. Flanigen. US Pat. 4310440 (1982); B.M. Lok, C.A. Messina, R.L. Oattib, R.T. Gatek, T.R. Cannan and E.M. Flanigen. US Patent 1 440 871 (1984).
6. J.M. Bennet, J.P. Cohen, E.M. Flanigen, J.J. Pluth and J.V. Smith. ACS Symp. Ser. 218, 109 (1983).
7. C.S. Blackwell and R.L. Patton. J. Phys. Chem. 88, 6135 (1984).
8. D. Goldfarb, J.-M. Fauth, Y. Tor and A. Shanzer. J. Am. Chem. Soc. 119, 1941 (1991).
9. J.-M. Fauth, A. Schweiger, L. Brauschweiler, J. Forrer, and R.R. Ernst. J. Mag. Reson. 66, 74 (1986).
10. V.V. Kurshev, A.M. Raitsimring and Y.D. Tsvetkov. J. Mag. Reson. 81, 441 (1989).
11. D. Goldfarb and K. Zukerman. Chem. Phys. Lett. 171, 168 (1990).
12. W.J. Mortier. Compilation of Extraframework Sites in Zeolites, Butterwork, Guildford (1982).
13. D.R. Taylor, J. Owen and B.M. Wanklyn. J. Phys. C.: Solid State Phys. 6, 2592 (1973).
14. T. Ichikawa and L. Kevan. J. Am. Chem. Soc. 103, 5355 (1981).
15. E.J. Reijerse, N.A.J. van Earle and C.P.J. Keijzers. J. Magn. Reson. 67, 114 (1986).
16. H.L. Flanagan, G.J. Gerfen, A. Lai and D.J. Singel. J. Chem. Phys. 88, 2162 (1987).
17. W.B. Mims. Phys. Rev. B 5, 2409 (1972).
18. Z. Luz and A.J. Vega. J. PHys. Chem. 91, 374 (1986).
19. J.M. Bennet, J.P. Cohen, E.M. Flanigen, J.J. Fluth and J.V. Smith. ACS Symp. Ser. 218, 109 (1983).
20. L. Kevan, M.K. Bowman, P.A. Narayana, R.K. Boekman, V.F. Yudonov and Yu.D. Tsnetkov. Chem. Phys. 63, 409 (1975).
21. Z. Levi, A.M. Raitsimring and D. Goldfarb. J. Phys. Chem. (in press).
22. J.R. Klander and P.W. Anderson. Phys. Rev. 125, 912 (1962).